Journal of Luminescence 195 (2018) 79–86

Contents lists available at ScienceDirect

Journal of Luminescence

journal homepage: www.elsevier.com/locate/jlumin

Electronic structure and optical properties of boron difluoride naphthaloyl- and anthracenoylacetonates

Sergey A. Tikhonov[a,*], Vitaliy I. Vovna[a], Igor B. Lvov[a], Ivan S. Osmushko[a], Aleksandr V. Borisenko[c], Elena V. Fedorenko[b], Anatoliy G. Mirochnik[b]

[a] Far Eastern Federal University, Vladivostok 690950, Russia
[b] Institute of Chemistry, Far Eastern Branch of the Russian Academy of Sciences, Vladivostok 690022, Russia
[c] Vladivostok Branch of Russian Customs Academy, Vladivostok 690034, Russia

ARTICLE INFO

Keywords:
Electronic structure
Photoelectron spectroscopy
Absorption spectra
Luminescence spectra
Density functional theory
Boron difluoride β-diketonates

ABSTRACT

Electronic structure and optical properties of boron difluoride naphthaloyl- (I) and anthracenoylacetonates (II) have been studied by the methods of photoelectron, absorption, luminescence spectroscopy as well as by quantum chemistry (DFT and TDDFT). In contrast with compound (I), the correlation of energies and types of transitions in excited states between compound (II) and anthracene molecule are ascertained. In addition, the bathochromic shift of the luminescence band maximum and decrease of luminescence quantum yield are detected. The decrease of luminescence quantum yield correlates with the reduction of C-C bond order between chelate ring and substituting group and with the decrease of the excited state lifetime. The good agreement between UV/X-ray photoelectron spectra data and Kohn-Sham orbital energies and structure confirms the reliability of the results of quantum-chemical modeling.

1. Introduction

Boron difluoride β-diketonates have intensive luminescence in the visible and near-IR range [1–6], ability to form excimers [7,8] and exciplexes [9,10], luminescence thermochromism [11] and liquid-crystal polymorphism [12–15]. These compounds are used as laser dyes [16], organic light-emitting diodes [17,18], optical chemosensors [19–21], active components of sunlight collectors [22], materials for non-linear optics [23] and polymer optical materials [24,25]. The investigation of the electronic structure of boron difluoride β-diketonates and their spectral properties opens the possibility for direct synthesis of new luminescent material. The most reliable information on the electronic structure of chelates can be obtained by joint application of methods of ultraviolet photoelectron spectroscopy (UPS), X-ray photoelectron spectroscopy (XPS) and quantum chemistry. Comparison of ionization energies obtained from photoelectron spectra [26], with the energies of Kohn-Sham (KS) molecular orbitals, makes it possible to reveal the features of the electronic structure of the systems under study.

A good correlation of the experimental and theoretical ionization energies indicates the reliability of the results of quantum-chemical modeling. The usage of the methods of absorption and luminescent spectroscopy in conjunction with the results of calculations in the approximation of the nonstationary density functional theory (TDDFT) makes it possible to establish relationships between the molecular design and the optical properties of boron difluoride complexes on the basis of analysis of substitution effects.

In [27–31], we showed that the results of calculations of the electronic structure of boron β-diketonate complexes in the DFT and TDDFT approximations correlate well with the experimental results obtained by photoelectron and optical spectroscopy. This makes it possible to exactly interpret photoelectron and optical spectra, as well as to analyze electronic substitution effects.

Earlier [27,28], we investigated the electronic structure and optical properties of boron difluoride dibenzoylmethanate and its four derivatives using XPS, absorption spectroscopy, luminescent spectroscopy, and DFT/TDDFT calculations. At present, there are no other publications devoted to a detailed study of the electronic structure of boron difluoride β-diketonates, which determines their luminescent properties.

The interest in the research of naphthaloyl (I) and anthracenoylacetonates (II) of boron difluoride is determined by their luminescent properties [32] and the prospect of creating new functional materials for phase holograms and integrated optical elements [33].

In this paper, we present the results of an investigation of the electronic structure and optical properties of compounds I-II (Scheme 1)

* Corresponding author.
E-mail address: allser@bk.ru (S.A. Tikhonov).

https://doi.org/10.1016/j.jlumin.2017.11.025
Received 17 July 2017; Received in revised form 17 October 2017; Accepted 13 November 2017
Available online 20 November 2017

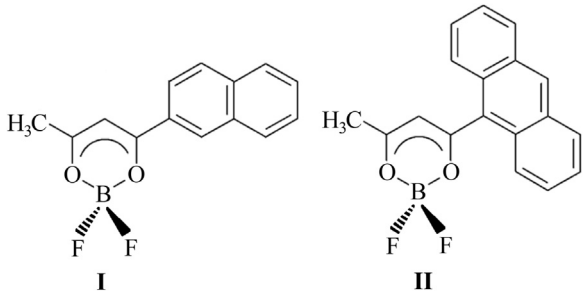

Scheme 1. Chemical structure of compounds I and II.

according to the methods of UPS, XPS, absorption spectroscopy, luminescence spectroscopy, and the results of calculations in the DFT and TDDFT approximations.

2. Experimental and calculation methods

Compounds I and II were prepared and purified according to [8,32] correspondingly. The absorption spectra were registered using a Shimadzu-UV2550 spectrometer (Japan). Anthracene solution used as a standard for measuring the fluorescence quantum yield (φ_F = 0.27) [34]. The measurements of fluorescence lifetime by time-correlated single-photon counting (TCSPC) were performed using a FluoTime 200 device (PicoQuant, Germany) with a LDH-P-C-375 (370 nm) excitation source and a TimeHarp device as the SPC controller. The lifetime data were analyzed using the FluorFit 4.0 software from PicoQuant. Chloroform was purchased from Roshimreaktiv and used as received.

UPS spectra of compounds I and II in a vapor phase were obtained on a modified electronic spectrometer ES-3201 with hemispherical electrostatic analyzer using monochromatic irradiation source He I ($h\nu$ = 21.2 eV). To calibrate spectra, xenon was used. The error in determining the band maxima did not exceed 0.02 eV. The temperature of the ionization cuvette depended on the sublimation temperature of the vapor and was in the range from 200 to 240 °C.

To compare the experimental values of vertical ionization energies (IE) with KS orbital energies ε_i we used a procedure similar to the extended Koopmans' theorem:

$$IE_i = \varepsilon_i + \delta_i,$$

where

IE_i — ionization energy;
ε_i — single-electron KS-energy;
δ_i — defect of density functional theory approximation (DFA-defect), which reflects the deviation of calculated single-electron energy ε_i from experimental vertical IE_i.

XPS spectra of molecular crystals of I and II were recorded by using a high-vacuum photoelectron spectrometer (Omicron, Germany) with a hemispherical electrostatic analyzer using a monochromatic radiation source MgKα ($h\nu$ = 1253.6 eV). The apparatus function of the spectrometer in the mode of recording of the characteristic levels of atoms, determined from the contour of the Ag $3d_{5/2}$ band, had a width at half-height of 1.2 eV. The calibration of the electron binding energy scale (E_b) is performed by the internal standard technique, which is the level of F 1 s (686.0 eV). When determining the atomic concentration of elements in the sample, the relative ionization cross sections and the photoelectron escape depth were taken into account. The relative concentrations of elements, obtained from the band intensities of 1s-electron, coincided with the calculated values by taking into account the method error (10%).

The bands of the XPS spectra of the valence and core levels are interpreted taking into account the number of calculated electronic levels, the energy intervals between them and the relative ionization cross sections.

The calculation method was chosen based on a good correlation between the experimental and theoretical ionization energies [31]. This is explained by the similarity of the Kohn-Shem equation and the Dyson quasiparticle equation. It was shown in [35,36], that in the valence region the KS orbitals can act as a good approximation to the Dyson orbitals. The general Dyson equation [37] is one of the methods for obtaining the Green's functions [38]. DFT and TDDFT calculations were performed using Firefly 8.1.G [39] and TZVP basic set [40,41]. The calculation results depend on the type of exchange-correlation functional. Now the hybrid [42], double-hybrid [43], Minnesota [44] and range-separated functionals [45,46] are used for DFT calculations. The method of dispersion correction as an add-on to standard KS density functional theory [47] is also used. The hybrid three-parameter B3LYP functional is successfully used for DFT calculations of boron complexes [48–54]. In our review [31] it was shown that hybrid B3LYP functional [55–57] gives good results for investigation of the electronic structure of boron complexes by UPS and XPS methods. Therefore, in this paper all calculations were performed using the B3LYP functional.

To interpret the optical spectra, the results of TDDFT calculations were used. To cover excited states up to vacuum ultraviolet energies (~8 eV), 50 electronic transitions for compounds I-II, naphthalene and anthracene were calculated. The calculated spectra are obtained from the values of the energies (E_i) and oscillator strengths (f_i) by summing the Gaussian curves $G_i(E) = a(f_i/d)\exp(-{}^1/_2(E-E_i)^2/d^2)$, where a is a factor to transform to the units of the molar extinction coefficient; i is the sequence number of the transition; d is the half-width parameter.

3. Results and discussion

3.1. Modeling of electronic structure

Optimization of the geometric parameters of I and II resulted in a slight (the few degrees) break in the plane of the chelate ring along the O-O line. For compound I, the violation of the coplanarity of the planes of the chelate ring and the substituent is 7°. In complex II, due to repulsion between hydrogen atoms in the γ-position of the chelate ring and at positions 1 and 8 of the anthracene fragment, the dihedral angle between the planes of the aromatic substituent and the chelate ring is 57°.

Fig. 1 shows the shapes of some molecular orbitals of compounds I and II. Table 1 shows the calculated molecular level energies ($-\varepsilon_i$) and the experimental ionization energies (IE_i) of compounds I and II according to the UPS method. The types of KS highest occupied molecular orbitals (MO) are determined from the contributions of Mulliken atomic populations, and for vacant MOs by the relative sum of the squares of the coefficients of the basic orbitals. π-Orbitals are conventionally divided into localized mainly on: chelate ring *a* (F_2B-O-C-CH-C-O-) and substituents *b* (naphthyl, anthryl). The delocalized MOs are conditionally designated as "*ab*" or "*ba*", depending on the prevailing localization. Orbitals *a* and *b* are considered mixed if the sum of the Mulliken atomic populations for each of the fragments is greater than 20%.

In order to interpret the ultraviolet and X-ray photoelectron spectra of compounds I and II, the structure of the valence and core levels was analyzed. To demonstrate electronic substitution effects, Fig. 2 shows a correlation diagram of the calculated levels of compounds I and II, naphthalene, anthracene and boron difluoride acetylacetonate (BF_2Acac). In compound I, the highest occupied molecular orbital (HOMO) is localized predominantly on a substituent (Table 1, Figs. 1 and 2b). Next are the antibonding and bonding combinations of the π_4-orbitals of the naphthyl group and π_3 of the chelate ring, as well as the π_3 and n-MOs of chelate rings (Fig. 2). In compounds I and II, the chelate ring stabilizes the orbitals of the substituents by 0.2–0.6 eV (Fig. 2) due to both the decrease in the electron density in the substituents (0.08e for I, 0.04e for II) and the field effect caused by the positive charge of the carbonyl carbon atom.

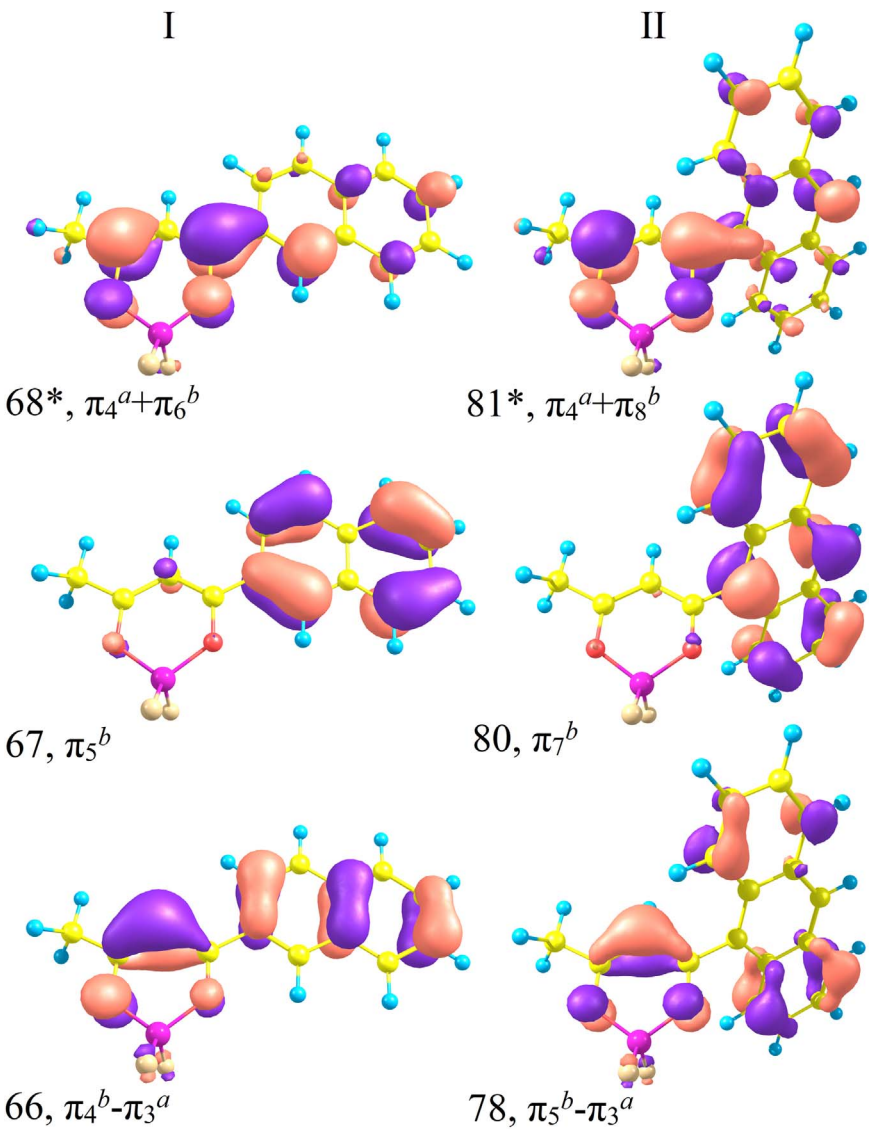

Fig. 1. Some molecular orbitals of the compounds I and II.

Table 1
Energy, type and localization of MOs on molecular fragments *a* and *b* for compounds I and II.

	MO	$-\varepsilon_i$, eV	type	Contribution (%)		IE, eV
				a	*b*	
I	70[a]	0.86	π_7^b-π_4^a	29	71	–
	69[a]	1.58	π_6^b	14	86	–
	68a	2.82	$\pi_4^a+\pi_6^b$	56	44	–
	67	6.60	π_5^b	7	93	8.40
	66	7.12	π_4^b-π_3^a	51	49	9.03
	65	7.72	$\pi_3^a+\pi_4^b$	55	45	9.64
	64	8.46	π_3^b	4	96	10.40
	63	8.74	n_-	89	11	10.92
II	84[a]	0.48	π_{10}^b	5	95	–
	83[a]	1.00	π_9^b	7	93	–
	82[a]	2.11	π_8^b-π_4^a	42	58	–
	81[a]	2.72	$\pi_4^a+\pi_8^b$	67	33	–
	80	5.88	π_7^b	7	93	7.56
	79	7.08	π_6^b	3	97	8.70
	78	7.36	π_5^b-π_3^a	45	55	9.20
	77	7.63	$\pi_3^a+\pi_5^b$	55	45	9.49
	76	8.64	n_-^a-π_4^b	56	44	10.64
	75	8.68	$\pi_4^b+n_-^a$	33	67	10.22
	74	8.78	π_3^b	5	95	10.45

[a] Vacant MO.

In the complexes studied, the energy levels of C 1s electrons are split, as in the case of dibenzoylmethanate of boron difluoride [27]. Depending on the energy value, the C 1s-electron levels are divided into two groups. 1s-Levels of carbonyl carbon atoms are designated as C 1s (β), and 1s-levels of other carbon atoms are designated as C 1s. The calculated difference in the energies of the C 1s levels of compounds I and II differs insignificantly (Fig. 2c, Supplementary material).

Optical properties of the complexes depend on characteristics of the valence levels considered above and the vacant MOs. From the calculations (Figs. 1 and 2a, Table 1) one can see the vacant MO structure of the studied compounds. π_4-Orbital of the chelate ring in complex I mixes with π_6 and π_7-orbitals of naphthyl group (Fig. 2a). π_4-MO of chelate ring in compound II mixes with π_8-MO of the substituent. In the transition from I to II, the destabilization of the HOMO level is observed, which leads to a decrease of HOMO-LUMO energy gap by 0.62 eV (Table 1).

3.2. Photoelectron spectra

In order to check the accuracy of the reproduction of the IE values of the condensed aromatic molecules in the DFT approximation, the experimental values of IE for naphthalene [58] and anthracene [59] are compared with the calculated electron energies corrected for the DFA defect (Table 2). The magnitude of the corrections to the orbital

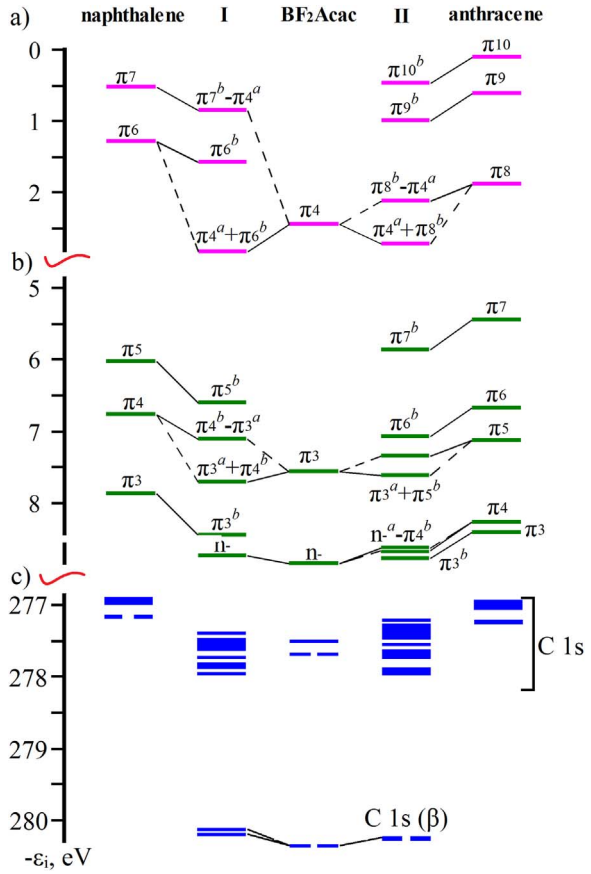

Fig. 2. MO energy diagram (DFT, B3LYP). Data in the columns are presented for naphthalene, I, BF_2Acac, II, anthracene (left to right). The electron levels: lower vacant (a), occupied (b) and C 1s (c). The lines of correlation join MOs of a similar type.

Table 2
Experimental [58,59] and calculated IE for naphthalene and anthracene.

Naphthalene	MO	π_5	π_4	π_3	π_2	-
	IE, eV	8.13	8.98	10.08	11.03	-
	$-\varepsilon_i+2.13$ eV	8.15	8.90	10.01	11.15	-
Anthracene	MO	π_7	π_6	π_5	π_4	π_3
	IE, eV	7.47	8.52	9.23	10.27	10.40
	$-\varepsilon_i+1.98$ eV	7.44	8.66	9.12	10.25	10.40

energies of the two molecules differ by 0.15 eV, which is explained by the decrease in the average value of the DFA-defect with increasing density of electronic states, caused by an increase in the number of atoms in molecular systems [31,60]. The maximum discrepancy between the theoretical and experimental values of IE for naphthalene and anthracene is 0.14 eV (Table 2). The maximum discrepancy between the theoretical and experimental values of IE for naphthalene and anthracene is 0.14 eV (Table 2). Taking into account the good correlation of the energy of the electron levels shown by the example of 11 boron β-diketonates [31], it is also possible to expect good agreement between the theoretical and experimental data for compounds I and II.

For complexes I and II, the results of calculations are compared with the UPS method data (Fig. 3, Table 1). In the spectra of both compounds, there is a fine band structure (1 in Fig. 3) due to the C=C-binding $\pi 5^b$- and $\pi 7^b$-orbitals, which is also observed in the molecules of naphthalene [58] and anthracene [59]. All five bands in the spectrum of compound I are caused by one-electron ionization process. Band 2 in the spectrum of compound II is caused by photoionization processes from one-electron level, and bands 3 and 4 correspond to two and three MOs.

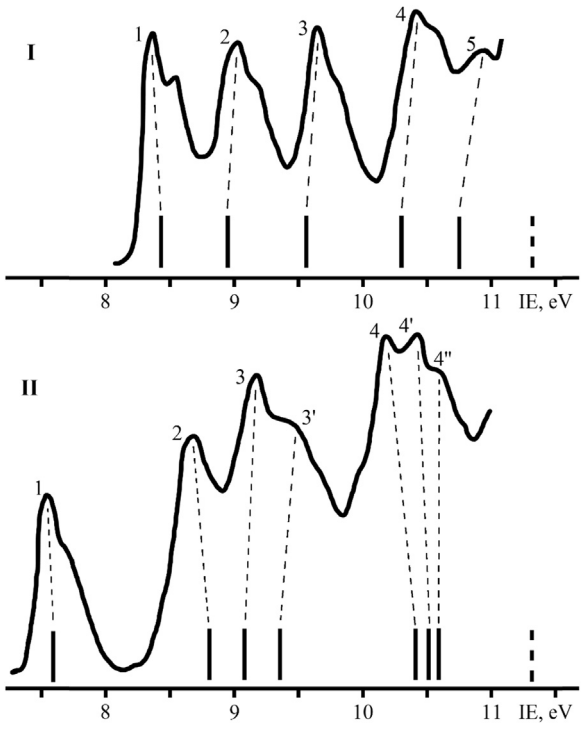

Fig. 3. UPS spectra of compounds I and II in vapor phase. Vertical lines correspond to calculated electron energies shifted by DFA-defect value. Dashed lines denote the nearest calculated electronic levels, for which IEs have not been identified.

The mean values of the DFA-defect for compounds I and II are 1.70 and 1.99 eV, respectively. By analogy with other β-diketonates of boron difluoride [31], the DFA-defect value of n-MOs of the investigated complexes is increased by 0.2 eV. The maximum discrepancy between experimental and theoretical IEs for 12 electronic levels of compounds I and II is 0.19 eV.

In order to obtain information on the lower valence and core levels, the results of calculations of the complexes I and II are compared with the XPS spectra. In the XPS spectra of the valence region of compounds I and II, three intensity maxima are observed in the energy range from 3 to 23 eV and two maxima at 27 and 31 eV (Fig. 4). The relative intensities and contours of the components are determined by the distribution of the density of electronic states and the relative ionization cross sections of the 2s- and 2p-levels (σ_s, σ_p). For Mg Kα source the σ_s:σ_p ratio for carbon is 13.3, for oxygen is 5.3 and for fluorine is 3.9, while the ratio σ_p(C): σ_p(O): σ_p(F) is 1.0: 6.0: 19.6 [60].

When interpreting the spectra of the valence region of compounds I and II, a technique was used that was previously used to analyze the XPS spectrum of BF_2Dbm and its derivatives [27,28]. In XPS spectra of complexes I and II, the maxima at 31 and 27 eV are due to ionization from the levels of F 2s and O 2s (Fig. 4). It was shown in [27,28] that the discrepancy between the experimental data for the ionization intensities of the 2s-levels of oxygen and fluorine in the series of boron difluoride β-diketonates is determined by delocalization of the electron density on the chelate ring. O 2s-orbitals of investigated complexes are also O—C-binding.

According to the results of quantum-chemical modeling, the maxima 1 in the spectra of compounds I and II are mainly due to AO F 2p, as well as high density of C 2p and O 2p levels (Fig. 4). The bends 1' are determined by the n_-orbitals (O 2p) of the chelate ring. The maxima 2 correspond to the mixed levels of C 2p and C 2s, and the shoulders 2′ are mainly due to F 2p AO. The maxima 3 and the bends 3′ are caused by photoionization processes from the C 2s levels.

The XPS spectra of the C 1s electrons of compounds I and II (Fig. 5) are supplemented by the calculated energies determining the positions

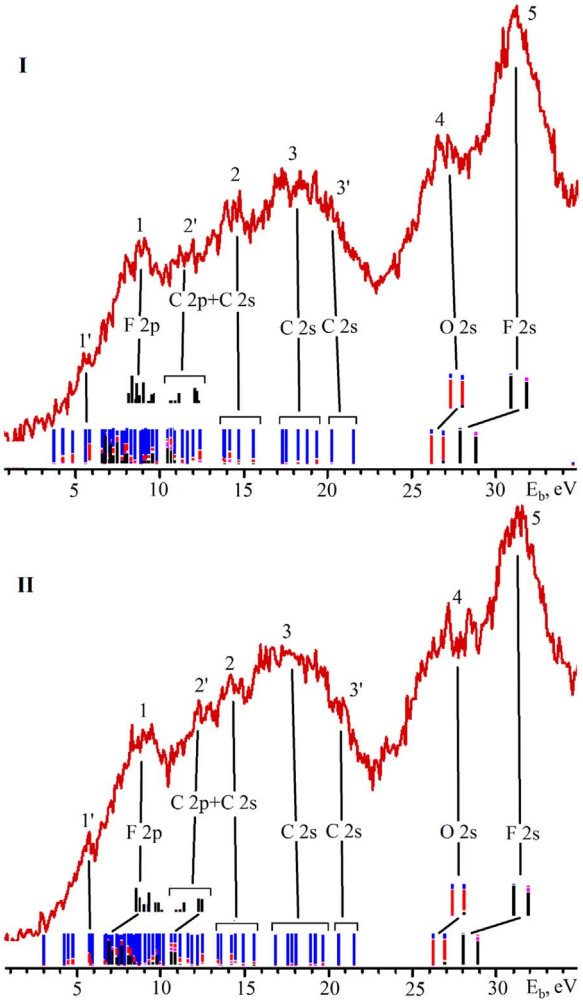

Fig. 4. XPS spectra of valence region of compounds I and II. The colored vertical lines correspond to calculated energies of MOs, localized mainly on carbon (blue), oxygen (red) and fluorine (black) atoms. The height of the vertical lines corresponds to the degree of contribution of atomic orbitals. Taking into account [27], the calculated energies of the orbitals localized on F and O atoms are shifted relative to the levels of C 2p and C 2s (O 2s — 1 eV, F 2s — 3 eV and F 2p — 1.5 eV).

Table 3
Energies and half-widths of bands in X-ray photoelectron spectra of 1s-electrons of complexes I and II.

Compd, electron levels	I		II	
	E_b	half-width	E_b	half-width
O 1s	532.9	2.2	532.8	2.4
C 1s	284.8	1.6	284.5	1.7
C 1s (C_β)	286.9	2.0	286.7	2.1
B 1s	193.8	1.6	193.8	1.6

*The binding energy E_b for F 1s-electrons of complexes I-II is 686.0 eV.

of the maxima of the 1s-electron bands in the binding energy scale E_b. In the XPS spectra of C 1s levels, good agreement between the energy differences and the relative areas of Gaussians with the calculated energies and the number of electronic levels is observed (Fig. 5). A satellite at 289 eV is commonly called "π-plasmon" [61] and associated with π → π* excitation of aromatic groups [62] (*shake-up* p_z-transition).

For both complexes, as for most boron difluoride β-diketonates [27,28], the binding energies of B 1s-electrons take on the values of 193.8 eV (Table 3), which, according to tabular data [26], is characteristic for a high oxidation state of boron atom.

3.3. Optical spectra

In order to interpret the absorption spectra of compounds I and II (Fig. 6), Table 4 presents the calculated characteristics of significant transitions in comparison with the experimental data of the absorption spectroscopy method. When determining the nature of the excited states described by the combination of several one-electron transitions, the relative contributions of each transition were taken into account. To determine the effect of substituents on the spectral-luminescent characteristics of the compounds I and II (Fig. 6), Table 4 presents the results of calculations of the excited states of naphthalene and anthracene.

For compounds I and II, there is a qualitative agreement between the experimental and calculated absorption spectra (Fig. 6). The exchange-correlation functional B3LYP used by us is successfully used in calculations of the electronic structure and for the interpretation of the optical spectra of boron complexes [48–54].

In the absorption spectrum of compound I two overlapping bands at 375 and 344 nm are caused by excited states 1 and 2 (Fig. 6a, Table 4).

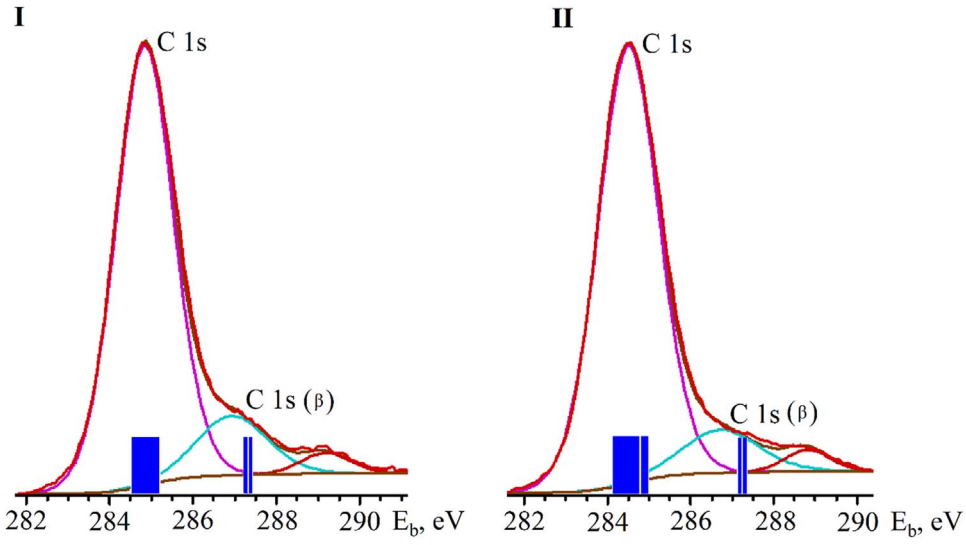

Fig. 5. XPS spectra of C 1s-levels of complexes I and II.

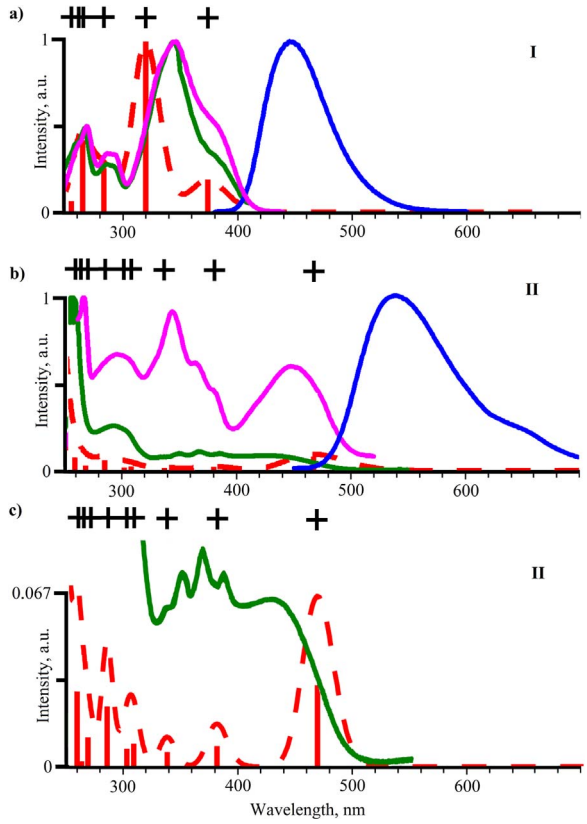

Fig. 6. Optical spectra of complexes I (*a*) and II (*b*). Experimental and theoretical absorption spectra of the compound II with the intensities being increased 15-fold (*c*). The experimental absorption spectra (green line), luminescence (blue line), and luminescence excitation (pink line). The theoretical absorption spectra are marked by the red dotted lines. The calculated energies of all states (crosses), energies of transitions depending on the oscillator strength (vertical red lines). For every compound, the types of transitions are designated that make the largest contribution to the intensity of the main absorption bands. (For interpretation of the references to color in this figure legend, the reader is referred to the web version of this article.)

The excited state no. 1 with the oscillator strength 0.103 is determined by the transition with electron density transfer (49%) from the substituent to the chelate ring. Unlike boron difluoride dibenzoylmethanate and its derivatives [27,28], in complex I the largest oscillator strength of 0.543 has a state corresponding to the second band. The bands at 286 and 266 nm correspond to the excited states 3 and 4–6, respectively. For complex I, there is a correlation of the types of transitions of excited states no. 1 and 6 with excited states no. 1 and 2 of naphthalene (Table 4). The difference in the transition energies is explained by the mixing of the π-orbitals of the substituent and the chelate ring. In particular, the stabilization of the HOMO level of compound I (the predominant contribution of π_4^a-orbital), in comparison with the HOMO level of naphthalene, leads to a decrease in the HOMO-LUMO energy gap by 0.96 eV, and a bathochromic shift of the long-wavelength absorption band.

In contrast to compound I, compound II is characterized by the presence of four transitions with significant electron density transfer. In particular, in the absorption spectrum of compound II (Fig. 6c), the bands at 432, 386 and 334 nm correspond to charge transfer transitions (60%, 35% and 64%) from the substituent to the chelate ring. The fine structure of the band at 386 nm is due to the vibrations of the C-C bonds of the substituent, which is also characteristic of the long-wave band in the absorption spectrum of anthracene (Table 4). The bands at 291 and 254 nm in the spectrum of complex II are determined by the excited states no. 4–6 and 7–12.

Energy and type of transitions of excited states no. 2, 5, 7, 9–11 in compound II correlate with the excited states no. 1–5 of anthracene. The mixing of the π_4-orbital of the chelate ring and the π_8-orbital of the substituent determines the decrease in the HOMO-LUMO energy gap of compound II by 0.41 eV in comparison with anthracene, which leads to a decrease in the energy of the excited state no. 1 and a bathochromic shift of the long-wave band of the absorption spectrum.

Unlike most boron β-diketonates [27,28], in the luminescence excitation spectra of compounds I and II, the bands in the short-wave interval of 320–350 nm are the most intense (Fig. 5b). These bands correspond to transitions between delocalized MOs (Table 4, Fig. 1). Probably, the possibility of a minimum redistribution of the electron density upon transition to the excited state promotes the activity of these transitions in the luminescence process.

The peculiarity of compound II is the nonplanar structure of its molecule: the aromatic substituent is unfolded relative to the plane of the chelate ring by 57° and must be weakly conjugated with its π-system. As a rule, the noncoplanar structure of the molecule of an organic compound should lead to a hypsochromic shift of the absorption and luminescence spectra with respect to analogues with a plane structure of the molecule. However, the luminescence spectrum of complex II is batochromically shifted as compared to compound I, the naphthyl group in which lies in the same plane as the β-diketonate ring (maxima of the luminescence spectra are at 538 and 448 nm, respectively). The shift of peak wavelength in the absorption and luminescence spectra is caused by reduction of HOMO-LUMO energy gap by 0.62 eV (Fig. 2, Table 1).

Luminescence quantum yield decreases from 0.53 (compound I) to 0.09 (compound II) (Table 5). The decrease in the relative quantum yield correlates with reduction of C-C bond order between the chelate ring and substituent, and a decrease in the lifetime of the excited state (Table 5). Decreasing of the rigidity of the molecule upon replacement of the naphthyl group with anthryl one determines the process of dissipation of the electronic excitation energy. In particular, for compound II, in comparison with complex I, a decrease in the order of the C-C bonds between the chelate ring and the substituent is observed, which can facilitate the rotation of the anthryl group upon excitation.

The large values of the Stokes shift for compounds I and II indicate charge transfer transitions, accompanied by a significant change in the geometry of the molecules during the transition to the first excited state.

4. Conclusion

For naphthaloyl- and anthracenoylacetonates of boron difluoride, compared with naphthalene and anthracene, there is a decrease in the HOMO-LUMO energy gap due to the mixing of π-orbitals of the substituents with the π_4-MOs of the chelate ring. This determines the bathochromic shift of the long-wave bands of the absorption spectra.

Analysis of the experimental and calculation results showed that, in contrast to the complex with a naphthyl group, a correlation of the energies and types of transitions of excited states no. 2, 5, 7, 9–11 with excited states no. 1–5 of anthracene is observed for the compound with the anthryl group. In particular, in boron difluoride anthracenoylacetonate, the fine structure of the second absorption band at 386 nm is due to the vibrations of the C-C bonds of the substituent. This is also characteristic of the long-wave band in the spectrum of anthracene.

Substitution of naphthyl group by anthryl one leads to a considerable increase of electronic charge transfer transitions from substituent to chelate ring and to a bathochromic shift of long wavelength band in the optical spectra. In addition, excited state lifetime shortens along with relative quantum yield value is reduced from 0.53 to 0.09 due to decrease of molecule's rigidity.

In the photoelectron spectra of the compounds studied, the structure of the upper valence levels, as well as the levels of O 1s, C 1s, F 2s, O 2s, C 2s and F 2p-electrons, agrees well with the results of quantum-chemical modeling, which confirms the reliability of the calculated data.

The obtained data can be used for the development of new optical

Table 4
Excited states in I-II, naphthalene and anthracene, calculated and experimental.

State (no.) Compound I	Transition	Type	λ, nm	*f*	exptl data, λ, nm	State (no.) Naphthalene	Transition	λ, nm	*f*	exptl data, λ, nm
1	$\pi_5^b \rightarrow \pi_4^a + \pi_6^b$ (92%)	*b-ab*	374	0.103	375	1	π_5-π_6 (94%)	284	0.056	288
2	π_4^b-$\pi_3^a \rightarrow \pi_4^a + \pi_6^b$ (85%)	*ba-ab*	320	0.543	344	-	-	-	-	-
3	$\pi_3^a + \pi_4^b \rightarrow \pi_4^a + \pi_6^b$ (60%)	*ab-ab*	283	0.139	286	-	-	-	-	-
	$\pi_5^b \rightarrow \pi_6^b$ (28%)	*b-b*								
4	$\pi_5^b \rightarrow \pi_6^b$ (50%)	*b-b*	265	0.229	266	-	-	-	-	-
	$\pi_3^a + \pi_4^b \rightarrow \pi_4^a + \pi_6^b$ (30%)	*ab-ab*								
5	$n_-^a \rightarrow \pi_4^a + \pi_6^b$ (91%)	*a-ab*	263	0.001		-	-	-	-	-
6	$\pi_5^b \rightarrow \pi_7^b$-$\pi_4^a$ (44%)	*b-ba*	255	0.035		2	π_5-π_7 (51%)	278	0.000	278
										268
	π_4^b-$\pi_3^a \rightarrow \pi_6^b$ (43%)	*ba-b*					π_4-π_6 (49%)			259
compound II						anthracene				
1	$\pi_7^b \rightarrow \pi_4^a + \pi_8^b$ (89%)	*b-ab*	467	0.105	432	1	π_7-π_8 (98%)	387	0.052	379
2	$\pi_7^b \rightarrow \pi_8^b$-$\pi_4^a$ (88%)	*b-ba*	380	0.026	386					
					367					360
					350					342
3	$\pi_6^b \rightarrow \pi_4^a + \pi_8^b$ (75%)	*b-ab*	336	0.018	334	-	-	-	-	-
4	π_5^b-$\pi_3^a \rightarrow \pi_4^a + \pi_8^b$ (85%)	*ba-ab*	307	0.029	291	-	-	-	-	-
5	$\pi_6^b \rightarrow \pi_8^b$-$\pi_4^a$ (58%)	*b-ba*	301	0.023		2	π_6-π_8 (51%)	321	0.000	326
	$\pi_7^b \rightarrow \pi_9^b$ (26%)	*b-b*					π_7-π_9 (49%)			
6	$\pi_3^a + \pi_5^b \rightarrow \pi_4^a + \pi_8^b$ (79%)	*ab-ab*	284	0.077		-	-	-	-	-
7	π_5^b-$\pi_3^a \rightarrow \pi_8^b$-$\pi_4^a$ (57%)	*ba-ba*	267	0.037	254	3	π_5-π_8 (57%)	274	0.000	
	$\pi_7^b \rightarrow \pi_{10}^b$ (25%)	*b-b*					π_7-π_{10} (42%)			
8	n_-^a-$\pi_4^b \rightarrow \pi_4^a + \pi_8^b$ (52%)	*ab-ab*	261	0.007		-	-	-	-	-
	$\pi_4^b + n_-^a \rightarrow \pi_4^a + \pi_8^b$ (27%)	*ba-ab*								
9	$\pi_7^b \rightarrow \pi_{10}^b$ (44%)	*b-b*	258	0.097		4	π_7-π_{10} (56%)π_5-π_8 (42%)	255	0.000	
	π_5^b-$\pi_3^a \rightarrow \pi_8^b$-$\pi_4^a$ (29%)	*ba-ba*								
10	$\pi_3^a + \pi_5^b \rightarrow \pi_8^b$-$\pi_4^a$ (64%)	*ab-ba*	248	0.104						
	$\pi_7^b \rightarrow \pi_{10}^b$ (21%)	*b-b*								
11	$\pi_7^b \rightarrow \pi_9^b$ (32%)	*b-b*	240	1.124		5	π_7-π_9 (51%)	239	1.986	
	$\pi_6^b \rightarrow \pi_8^b$-$\pi_4^a$ (23%)	*b-ba*					π_6-π_8 (49%)			
12	$\pi_7^b \rightarrow \pi_{11}^b + \pi_5^a$ (27%)	*b-ba*	239	0.501		-	-	-	-	-
	$\pi_4^b + n_-^a \rightarrow \pi_4^a + \pi_8^b$ (24%)	*ba-ab*								

Table 5
Long-wavelength maxima positions in absorption, excitation and luminescence spectra, Stokes shift values ν(ST), relative quantum yields φ, excited state lifetime τ, C-C bond order between chelate ring and substituent X for compounds I and II.

Compound	λ_{abs}, nm	λ_{ex}, nm	λ_{lum}, nm	φ	τ, ns	ν(ST), cm^{-1}	*X*, a.u.
I	375	378	448	0.53	1.9	4 346	1.11
II	432	449	538	0.09	0.9	4 562	1.03

functional materials based on boron compounds, which are promising for devices for converting and processing of optical signals, optical sensors, and optoelectronics.

Acknowledgements

This work was supported by the Ministry of Education and Science of the Russian Federation within the framework of project part of the state task (Project No. 3.2168.2017/4.6).

Appendix A. Supporting information

Supplementary data associated with this article can be found in the online version at https://doi.org/10.1016/j.jlumin.2017.11.025.

References

[1] D.-J. Wang, Y.-F. Kang, L. Fan, Y.-J. Hu, J. Zheng, Synthesis and photoluminescence behavior of difluoroboron complexes with β-diketone ligands, Opt. Mater. 36 (2013) 357–361.
[2] Y. Pi, D.-J. Wang, H. Liu, Y.-J. Hu, X.-H. Wei, J. Zheng, Synthesis and spectroscopic properties of some new difluoroboron bis-β-diketonate derivatives, Spectrochim. Acta Part A 131 (2014) 209–213.
[3] Y. Suwa, M. Yamaji, H. Okamoto, Synthesis and photophysical properties of difluoroboronated β-diketones with the fluorene moiety that have high fluorescence quantum yields, Tetrahedron Lett. 57 (2016) 1695–1698.
[4] C. Liu, H. Zhang, J. Zhao, Synthesis, characterization and properties of furan-containing difluoroboron complexes, RSC Adv. 6 (2016) 92341–92348.
[5] E.V. Fedorenko, A.G. Mirochnik, A.Y. Beloliptsev, New polymers containing BF2-benzoylacetonate groups. Synthesis, luminescence, excimer and exciplex formation, J. Lumin. 185 (2017) 23–33.
[6] H. Zhang, C. Liu, J. Xiu, J. Qiu, Triphenylamine-modified difluoroboron dibenzoylmethane derivatives: synthesis, photophysical and electrochemical properties, Dyes Pigm. 136 (2017) 798–806.
[7] A.G. Mirochnik, B.V. Bukvetskii, E.V. Gukhman, V.E. Karasev, Crystal structure and excimer fluorescence of some benzoylacetonatoboron difluorides: stacking factor, J. Fluoresc. 13 (2003) 157–162.
[8] B.V. Bukvetskii, E.V. Fedorenko, A.G. Mirochnik, A.Y. Beloliptsev, Crystal structure of boron difluoride 1-naphthylbutanedionate-1,3 (C10H7COCHCOCH3BF2). π-stacking interaction and luminescence, J. Struct. Chem. 51 (2010) 545–551.
[9] Y.L. Chow, C.I. Johansson, Exciplexes of (dibenzoylmethanato)boron benzenes: the control of exciplex electronic structure, J. Phys. Chem. 99 (1995) 17558–17565.
[10] Y.L. Chow, C.J. Johansson, Exciplex binding energy and kinetic rate constants of the interaction between singlet excited state dibenzoylmethanatoboron difluoride and substituted benzenes, J. Phys. Chem. 99 (1995) 17566–17572.
[11] A.G. Mirochnik, E.V. Fedorenko, B.V. Bukvetskii, V.E. Karasev, Reversible luminescence thermochromism of dibenzoyl(methanato)boron difluoride, Russ. Chem. Bull. 54 (2005) 1060–1062.
[12] O.A. Turanova, G.G. Garifzyanova, A.N. Turanov, Liquid crystal polymorphism of boron difluoride beta-diketonates, Rus. J. Gen. Chem. 80 (2010) 2317–2322.
[13] M.J. Mayoral, P. Ovejero, M. Cano, G. Orellana, Alkoxysubstituted difluoroboron benzoylmethanes for photonics applications: a photophysical and spectroscopic study, Dalton Trans. 40 (2011) 377–383.
[14] I. Sánchez, J.A. Campo, J.V. Heras, M. Cano, E. Oliveira, Liquid crystal behavior induced in highly luminescent unsymmetrical boron difluoride β-diketonate material, Inorg. Chim. Acta 381 (2012) 124–136.
[15] E. Giziroglu, A. Nesrullajev, N. Orhan, 1,3-Dimethyl-5-(3,4,5tris(alkoxy)benzoyl) barbituric acid derivatives and their liquid crystalline difluoroboron complexes: synthesis, characterization and comparative investigations of mesomorphic, thermotropic and thermomorphologic properties, J. Mol. Struct. 1057 (2014) 246–253.
[16] P. Czerney, G. Haucke, C. Igney, German patent (East) DD/265266. 1987, Chem. Abstr. 112 (45278) (1990).
[17] C.A. DeRosa, C. Kerr, Z. Fan, M. Kolpaczynska, A.S. Mathew, R.E. Evans, G. Zhang, C.L. Fraser, Tailoring oxygen sensitivity with halide substitution in difluoroboron dibenzoylmethane polylactide materials, ACS Appl. Mater. Interfaces 7 (2015) 23633–23643.
[18] M.L. Daly, C.A. DeRosa, C. Kerr, W.A. Morris, C.L. Fraser, Blue thermally activated delayedfluorescence from a biphenyl difluoroboron b-diketonate, RSC Adv. 6

(2016) 81631–81635.
[19] L. Zhai, M. Liu, P. Xue, J. Sun, P. Gong, Z. Zhang, J. Sun, R. Lu, Nanofibers generated from nonclassical organogelators based on difluoroboron β-diketonate complexes to detect aliphatic primary amine vapors, J. Mater. Chem. C 4 (2016) 7939–7947.
[20] A.S. Mathew, C.A. DeRosa, J.N. Demas, C.L. Fraser, Difluoroboron β-diketonate materials with longlived phosphorescence enable lifetime based oxygen imaging with a portable cost effective camera, Anal. Methods 8 (2016) 3109–3114.
[21] J. Samonina-Kosicka, D.H. Weitzel, C.L. Hofmann, H. Hendargo, G. Hanna, M.W. Dewhirst, G.M. Palmer, C.L. Fraser, Luminescent difluoroboron β-diketonate PEG-PLA oxygen nanosensors for tumor imaging, Macromol. Rapid Commun. 36 (2015) 694–699.
[22] M. Halik, G. Schmid, L. Davis, German patent 10152938, Chem. Abstr. 123 (378622) (2003).
[23] R. Kammler, G. Bourhill, Y. Jin, C. Bra¨uchle, G. Go¨rlitz, H. Hartmann, Second-order optical non-linearity of new 1,3,2(2H)dioxaborine dyes, J. Chem. Soc., Faraday Trans. 92 (1996) 945–947.
[24] K. Tanaka, K. Tamashima, A. Nagai, T. Okawa, Y. Chujo, Facile modulation of optical properties of diketonate-containing polymers by regulating complexation ratios with boron, Macromolecules 46 (2013) 2969–2975.
[25] G. Zhang, R.E. Evans, K.A. Campbell, C.L. Fraser, Role of boron in the polymer chemistry and photophysical properties of difluoroboron-dibenzoylmethane polylactide, Macromolecules 42 (2009) 8627–8633.
[26] S. Hu¨fner, Photoelectron Spectroscopy: Principles and Applications, Springer, Berlin, 1996.
[27] V.I. Vovna, S.A. Tikhonov, M.V. Kazachek, I.B. Lvov, V.V. Korochentsev, E.V. Fedorenko, A.G. Mirochnik, Electronic structure and optical properties of boron difluoride dibenzoylmethane F2Bdbm, J. Electron Spectrosc. Relat. Phenom. 189 (2013) 116–121.
[28] S.A. Tikhonov, V.I. Vovna, N.A. Gelfand, I.S. Osmushko, E.V. Fedorenko, A.G. Mirochnik, Electronic structure and optical properties of boron difluoride dibenzoylmethane derivatives, J. Phys. Chem. A 120 (2016) 7361–7369.
[29] V.I. Vovna, S.A. Tikhonov, I.B. Lvov, I.S. Osmushko, I.V. Svistunova, O.L. Shcheka, Photoelectron spectra and electronic structure of some spiroborate complexes, J. Electron Spectrosc. Relat. Phenom. 197 (2014) 43–49.
[30] S.A. Tikhonov, I.B. Lvov, V.I. Vovna, Photoelectron spectra and electronic structure of boron acetylacetonates with organic substituents, Russ. J. Phys. Chem. B 33 (2014) 11–18.
[31] I.S. Osmushko, V.I. Vovna, S.A. Tikhonov, Y.V. Chizhov, I.V. Krauklis, Application of DFT for the modeling of the valence region photoelectron spectra of boron and d-element complexes and macromolecules, Int. J. Quantum Chem. 116 (2016) 325–332.
[32] E.V. Fedorenko, B.V. Bukvetskii, A.G. Mirochnik, D.H. Shlyk, M.V. Tkacheva, A.A. Karpenko, Luminescence and crystal structure of 2,2-difluoro-4-(9-antracyl)-5-methyl-1,3,2-dioxoborine, J. Lumin. 130 (2010) 758–761.
[33] A.Y. Zhizhchenko, O.B. Vitrik, Y.N. Kulchin, A.G. Mirochnik, E.V. Fedorenko, G. Lv, A.M. Shalagin, V.P. Korolkov, Photoinduced record of wave guide structures in films of polymethylmethacrylate doped with beta-diketonatoborondifluorides, Opt. Commun. 311 (2013) 364–367.
[34] J.N. Demas, G.A. Crosby, Measurement of photoluminescence quantum yields, Rev. J. Phys. Chem. 75 (1971) 991–1024.
[35] S. Hamel, P. Duffy, M.E. Casida, D.R. Salahub, Kohn-Sham orbitals and orbital energies: fictitious constructs but good approximations all the same, J. Electron Spectrosc. Relat. Phenom. 123 (2002) 345–363.
[36] P. Duffy, D.P. Chong, M.E. Casida, D.R. Salagub, Assessment of Kohn-Sham density-functional orbitals as approximate Dyson orbitals for the calculation of electron-momentum-spectroscopy scattering cross sections, Phys. Rev. A: At., Mol., Opt. Phys. 50 (1994) 4707–4728.
[37] E.K.U. Gross, E. Runge, O. Heinonen, Many Particle Theory, Adam Hilger, Bristol, U.K., 1992.
[38] E.N. Economou, Green's Functions in Quantum Physics, Springer, New York, 1979.
[39] A.A. Granovsky, Firefly version 8.1.1.G. ⟨http://classic.chem.msu.su/gran/firefly/⟩ (Accessed 15 February 2017).
[40] Basis Set Exchange, version 1.2.2. ⟨https://bse.pnl.gov/bse/portal/⟩ (Accessed 15 February 2017), 2017.
[41] K. Eichkorn, F. Weigend, O. Treutler, R. Ahlrichs, Auxiliary basis sets for main row atoms and transition metals and their use to approximate Coulomb potentials, Theor. Chem. Acc. 97 (1997) 119–124.
[42] M. Marsman, J. Paier, A. Stroppa, G. Kresse, Hybrid functionals applied to extended systems, J. Phys.: Condens. Matter 20 (2008) 064201.
[43] L. Goerigk, S. Grimme, Double-hybrid density functionals, Wiley Interdiscip. Rev.: Comput. Mol. Sci. 4 (2014) 576–600.
[44] Y. Zhao, D.G. Truhlar, Applications and validations of the Minnesota density functionals, Chem. Phys. Lett. 502 (2011) 1–13.
[45] A.E. Raeber, B.M. Wong, The importance of short- and longrange exchange on various excited state properties of DNA monomers, stacked complexes, and Watson-Crick pairs, J. Chem. Theory Comput. 11 (2015) 2199–2209.
[46] A. Prlj, B.F.E. Curchod, A. Fabrizio, L. Floryan, C. Corminboeu, Qualitatively incorrect features in the TDDFT spectrum of thiophene-based compounds, J. Phys. Chem. Lett. 6 (2015) 13–21.
[47] S. Grimme, J. Antony, S. Ehrlich, H. Krieg, A consistent and accurate ab initio parametrization of density functional dispersion correction (DFT-D) for the 94 elements H-Pu, J. Chem. Phys. 132 (2010) 154104–154118.
[48] M.V. Kazachek, I.V. Svistunova, Excited states and absorption spectra of 2-β-diketonato-1,3,2-benzodioxaborol with aromatic substituents: quantum-chemistry modeling, Spectrochim. Acta Part A 148 (2015) 60–65.
[49] Y. Kubota, K. Kasatani, H. Takai, K. Funabiki, M. Matsui, Strategy to enhance solid-state fluorescence and aggregation-induced emission enhancement effect in pyrimidine boron complexes, Dalton Trans. 44 (2015) 3326–3341.
[50] M.-C. Chang, E. Otten, Reduction of (formazanate)boron difluoride provides evidence for an n-heterocyclic B(I) carbenoid intermediate, Inorg. Chem. 54 (2015) 8656–8664.
[51] S.N. Margar, L. Rhyman, P. Ramasami, N. Sekar, Fluorescent difluoroboron-curcumin analogs: an investigation of the electronic structures and photophysical properties, Spectrochim. Acta Part A 152 (2016) 241–251.
[52] M. Kolpaczynska, C.A. DeRosa, W.A. Morris, C.L. Fraser, Thienyl difluoroboron β-diketonates in solution and polylactide media, Aust. J. Chem. 69 (2016) 537–545.
[53] K. Kamada, T. Namikawa, S. Senatore, C. Matthews, P.-F. Lenne, O. Maury, C. Andraud, M. Ponce-Vargas, B.L. Guennic, D. Jacquemin, P. Agbo, D.D. An, S.S. Gauny, X. Liu, R.J. Abergel, F. Fages, A. D'Aleo, Boron difluoride curcuminoid fluorophoreswith enhanced two photon excited fluorescence emission and versatile living-cell imaging properties, Chem. Eur. J. 22 (2016) 5219–5232.
[54] H. Zhang, C. Liu, J. Xiu, J. Qiu, Triphenylamine-modified difluoroboron dibenzoylmethane derivatives: synthesis, photophysical and electrochemical properties, Dyes Pigm. 136 (2017) 798–806.
[55] C. Lee, W. Yang, R.G. Parr, Development of the Colle-Salvetti correlation-energy formula into a functional of the electron density, Phys. Rev. B: Condens. Matter Mater. Phys. 37 (1988) 785–789.
[56] A.D. Becke, Density-functional thermochemistry. III. The role of exact exchange, J. Chem. Phys. 98 (1993) 5648–5652.
[57] P.J. Stephens, F.J. Devlin, C.F. Chabalowski, M.J. Frisch, Ab initio calculation of vibrational absorption and circular dichroism spectra using density functional force fields, J. Phys. Chem. 98 (1994) 11623–11627.
[58] W.R. Moomaw, D.A. Kleier, J.H. Markgraf, J.W. Thoman, N.A. Ridyard, Photoelectron spectra and theoretical studies of bonding in strained quinolines, J. Phys. Chem. 92 (1988) 4892–4898.
[59] T. Kajiwara, S. Masuda, K. Ohno, Y. Harada, Application of Penning ionization electron spectroscopy to assignments of electron spectroscopic bands of anthracene, J. Chem. Soc. Perkin Trans. 2 (4) (1988) 507–511.
[60] J.J. Yeh, I. Lindau, Atomic subshell photoionization cross sections and symmetry parameters: $1 < Z < 103$, At. Data Nucl. Data Tables 32 (1985).
[61] N. Ooi, A. Rairkar, J.B. Adams, Density functional study of graphite bulk and surface properties, Carbon 44 (2006) 231–242.
[62] E.A. Taft, H.R. Phillipp, Optical properties of graphite, Phys. Rev. 138 (1965) A197.